Detection of Subclinical Keratoconus Using Biometric Parameters

Jose Sebastián Velázquez-Blázquez[1], Francisco Cavas-Martínez[1(✉)], Jorge Alió del Barrio[2,3], Daniel G. Fernández-Pacheco[1], Francisco J. F. Cañavate[1], Dolores Parras-Burgos[1], and Jorge Alió[2,3]

[1] Department of Graphical Expression, Technical University of Cartagena, 30202 Cartagena, Spain
francisco.cavas@upct.es
[2] Keratoconus Unit of Vissum Corporation Alicante, 03016 Alicante, Spain
[3] Department of Ophthalmology, Miguel Hernández University of Elche, 03202 Alicante, Spain

Abstract. The validation of innovative methodologies for diagnosing keratoconus in its earliest stages is of major interest in ophthalmology. So far, subclinical keratoconus diagnosis has been made by combining several clinical criteria that allowed the definition of indices and decision trees, which proved to be valuable diagnostic tools. However, further improvements need to be made in order to reduce the risk of ectasia in patients who undergo corneal refractive surgery. The purpose of this work is to report a new subclinical keratoconus detection method based in the analysis of certain biometric parameters extracted from a custom 3D corneal model.

This retrospective study includes two groups: the first composed of 67 patients with healthy eyes and normal vision, and the second composed of 24 patients with subclinical keratoconus and normal vision as well. The proposed detection method generates a 3D custom corneal model using computer-aided graphic design (CAGD) tools and corneal surfaces' data provided by a corneal tomographer. Defined bio-geometric parameters are then derived from the model, and statistically analysed to detect any minimal corneal deformation.

The metric which showed the highest area under the receiver-operator curve (ROC) was the posterior apex deviation.

This new method detected differences between healthy and sub-clinical keratoconus corneas by using abnormal corneal topography and normal spectacle corrected vision, enabling an integrated tool that facilitates an easier diagnosis and follow-up of keratoconus.

Keywords: Ophthalmology · Early keratoconus · Computational modelling · Scheimpflug technology

1 Introduction

Debilitating primary corneal ectasia shows changes in the corneal structure, including stromal thinning and progressive change of shape related to breakage of Bowman's membrane [1]. These morphological changes seriously affect the rigidity and elasticity

I. Rojas et al. (Eds.): IWBBIO 2019, LNBI 11466, pp. 490–501, 2019.
https://doi.org/10.1007/978-3-030-17935-9_44

of the tissues that form part of the corneal surface and behave very sensitively to variations in intraocular pressure [2]. Corneal shape shows changes such as conical focal corneal deformation located in the central or paracentral region [3]. This is followed by a progressive myopization, astigmatic shift with irregular astigmatism and progressive visual loss [4]. This disease usually begins in puberty and progresses to the third or fourth decade of life [5].

Several systems have been described in the literature for diagnosing and classifying keratoconus (KC) severity. Most of these grading systems have been developed by considering the patient's optical and geometric parameters [2, 31]. These systems have proven essential as a therapeutic approach to manage keratoconus [6].

A sample of this disease with a located steepening pattern exists, but neither clinical signs of the disease, nor other causes that could explain an altered topographical pattern, are manifested, and patients present the sharpness of normal visual correction. Subclinical keratoconus was a term introduced by Amsler [7] and is a condition in which the clinician suspects the potential clinical development of keratoconus. Identifying keratoconus in early stages is crucial to monitor disease progression [6, 8, 9], to perform genetic studies with the patient [10], to indicate therapeutic approaches to avoid its evolution [11], even most importantly, when making the preoperative screening of candidates for refractive surgery. The last reason has been identified as one of the main risk factors for ectasia after LASIK, after PRK [6–10], and even after low myopic ablations [12], because refractive surgery can weaken corneal tissues, and failure can be detected in cornea's biomechanics in totally asymptomatic individuals [13]. For these reasons, it is a fundamental challenge for the ophthalmic community to improve the strategies, tools and techniques employed to detect those individuals at potential risk of developing this pathology.

So far, subclinical keratoconus diagnosis has been made by combining several clinical criteria: age, family history, genetic predisposition [7] and corneal topography [14]. The topographic data and optical parameters obtained in this way have defined univariate and multivariate indices for detection, and for the decision trees or neural networks based on these indices, now valuable tools for detecting subclinical keratoconus [9, 15, 32].

However, further improvements should be made to detect subclinical keratoconus in order to enhance the strategies that diagnose this disease and to avoid the risk of ectasia in patients who undergo corneal refractive surgery. Progression from subclinical to clinical keratoconus is more likely to occur in patients aged 10–20 years, and is less likely to occur in patients over the age of 30 [7]. These cases are difficult to diagnose because symptoms are lacking in early disease stages. When patients come to consultations, the disease may have already advanced to the clinical keratoconus stage. Many studies are attempting to find an objective way to detect these cases and to treat them before their visual function is affected [11].

Accordingly, a subclinical keratoconus detection technique could be based on analysing the biometric morphometry of discrete landmarks [16] in the region where the focused curvature was initially manifested on corneal surfaces, because no other clinical signs are observed in this stage and patients present normal corrected visual acuity. In the biology and modern medicine fields, a geometric morphometric analysis works on a multidimensional image of a discrete data set obtained from a three-

dimensional reconstruction of biological structures [17]. These studies are characterized by both high sensitivity and specificity for structure characterization or pattern recognition, regardless of the technology used to generate the virtual model. This procedure could prove to be a methodological analysis process because the virtual environment provides a large number of hypotheses, which can avoid using complex analytical methods and can considerably reduce in vivo experimentation costs [17].

We have previously demonstrated that morphogeometric analysis of a custom virtual model of the cornea could be useful for the study of keratoconus characterization, and has been previously validated for the evaluation of disease progression across its different clinical stages [18, 19]. It has also been recently used in ophthalmology, specifically in the cornea biomechanics field, where some authors propose a customized model of the cornea obtained from interpolating the topographic data, which is further used as a basis for biomechanical analyses [20–22].

The aim of this study is to provide new rational and objective indices that accurately quantify the morphogeometric changes associated to the clinical evidence of corneal ectatic disease, enabling the description of early local ectasia in a preclinical stage, and to allow healthy corneas to be differentiated from corneas with the so-called subclinical keratoconus in order to avoid idiopathic progression of the disease.

2 Materials and Methods

2.1 Participants

This observational case series study evaluated 91 subjects (only one cornea per patient, randomly selected to avoid interference) divided into two groups: the first group (healthy corneas) presented no ocular pathology and included 67 patients (36.51 ± 14.99 years). In the second group were included 24 patients diagnosed with subclinical keratoconus (33.99 ± 10.97 years). Participants with any kind of ocular pathology were excluded from both groups.

The classification protocol for normal or subclinical keratoconus cases was run according to reported state of the art of clinical and topography evaluations [23].

These evaluations were made in Vissum Hospital (Alicante, Spain). The study follows ethical standards of the Declaration of Helsinki and was approved by the local Clinical Research Ethics Committee with informed consent.

2.2 Examination Protocol

Examination of all the selected patients was performed following a previous validated protocol created by our research group and using Sirius System® (CSO, Florence, Italy) [18, 19]. In this protocol, only the data from the first stage of the tomographic data acquisition procedure, so called raw data, is registered. Using the tomographer's vision algorithm in this first stage, we obtained a finite set of discrete, real and representative spatial data from the corneal surfaces [18, 19]. For obtaining the average values that were used for later analyses, a set of three successive measures were taken, always by the same expert optometrists.

2.3 Detection Procedure

The procedure proposed in this article consisted in two stages: first, using raw data from the corneal tomographer, a virtual 3D model was reconstructed throughout computational geometry techniques; second, geometric parameters were determined from this model and analysed in order to characterize the cornea morphology.

First Stage: Virtual 3D Modelling

The reconstruction of the cornea was performed by following the steps below (Fig. 1):

(i) *Acquisition of data from the corneal tomographer.*

The Syrius device provides two 3D point clouds that make up both the anterior and the posterior corneal surface, respectively (see Fig. 1). With this procedure we obtained useful data avoiding the interpolation that manufacturers use to fill or substitute wrongly scanned data [24].

We have taken into account that major irregularity levels in the corneal morphology of keratoconic eyes for both the corneal surfaces were presented between radii of 0–4 mm, which encompasses 97% of all keratoconus cases [25]. Any case in which the data provided by the Sirius tomographer had some erroneous point in the study area (r = 0–4 mm) was discarded.

Spatial points for both surfaces are obtained in polar format. These points are distributed in regular circles (256 points for each circle) in the XY plane whose radii are incremented in intervals of 0.2 mm. [18, 19]. To proceed with the reconstruction process, points' elevation data were then converted to Cartesian coordinates (X, Y, Z) using the following equations:

$$X = 0.2i \cdot \cos\left(j\frac{360^\circ}{256}\right);\ Y = 0.2i \cdot \sin\left(j\frac{360^\circ}{0256}\right);\ Z = \text{value in the exported table} \tag{1}$$

For this study, an algorithm programmed in Matlab V R2015 (Mathworks, Natick, USA) was implemented to perform this task.

(ii) *Geometric Surface Reconstruction and Solid Modelling.*

In a second stage, after the conversion of the spatial points into a Cartesian format, data were imported to the surface reconstruction CAD software Rhinoceros® V 5.0 (MCNeel & Associates, Seattle, USA). Non-uniform rational B-splines were used to generate surfaces applying point grid function, which allows a fitting of the reconstructed surface with regard to the point cloud of about 4.91 × 10–16 ± 5.19 × 10–16 mm.

The generated surface was then imported into the software SolidWorks V 2017 (Dassault Systèmes, Vélizy-Villacoublay, France), which allowed the generation of an in vivo solid model representing the custom biometrics of each cornea.

Second Stage: Biometric Parameters Analysis

The final 3D virtual model of the cornea was then used to run an analysis of the determined biometric parameters. These geometric parameters studied herein, along

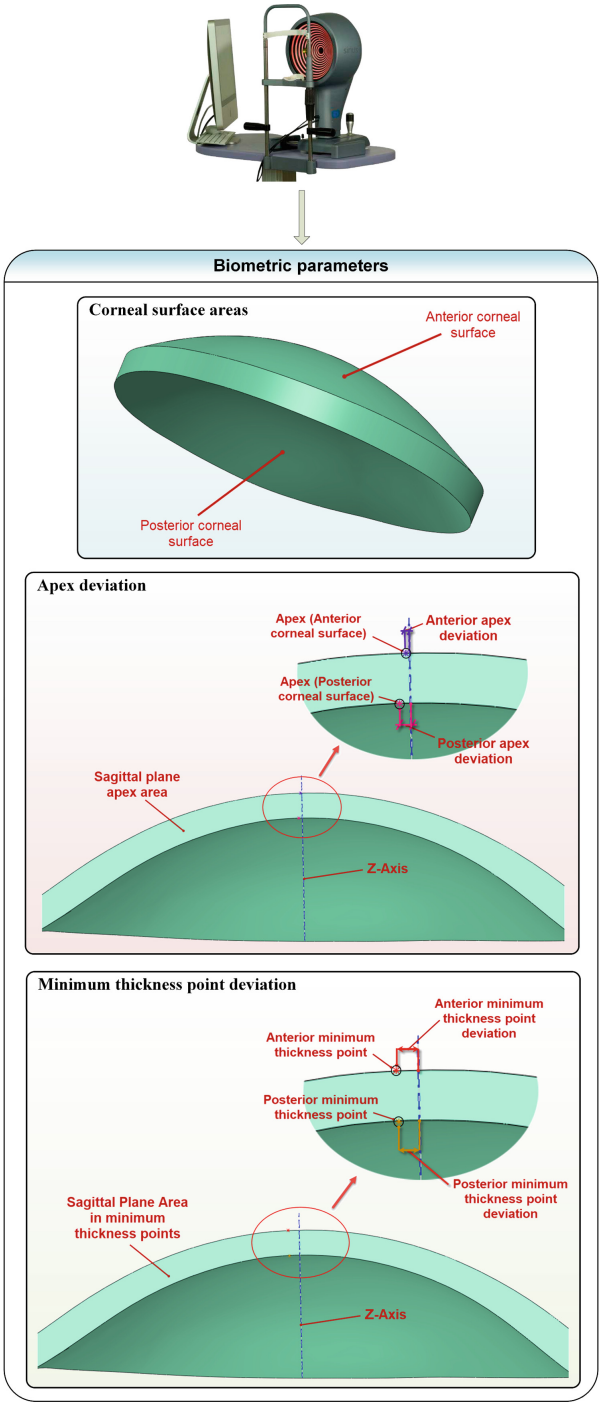

Fig. 1. Corneal surface areas, apex deviation and minimum thickness point deviation

with their characteristics have been previously described [19], and are shown in Table 1, being used in this case for the first time to detect subclinical keratoconus.

2.4 Statistical Analysis

A Kolmogorov-Smirnov test was run to assess the data engagement scores. According to this test and thereafter, a Student's t-test or U-Mann Whitney Wilcoxon test was employed, as and when appropriate. ROC curves were established to determine what parameters could be used to classify the diseased corneas by calculating optimal cut-offs, sensitivity and specificity [26, 27]. All the analyses were performed by the Graphpad Prism V 6 (GraphPad Software, La Jolla, USA) and SPSS V 17.0 software (SPSS, Chicago, USA).

3 Results

Most of the modelled parameters showed statistically significant differences when comparing healthy and subclinical corneas, as shown in Table 1 below.

Table 1. Descriptive values and differences in the modelled biometric parameters among the normal and subclinic KC groups (SD: standard deviation, P: statistical test, Z: z-score).

Biometric parameters	Normal group (n = 67)				Subclinical KC group (n = 24)				Z	P
	Mean	SD	Min	Max	Mean	SD	Min	Max		
Total corneal volume (mm^3)	25.80	1.57	21.29	29.39	24.09	1.69	19.79	28.21	–8.39	0.00
Anterior corneal surface area (mm^2)	43.10	0.16	42.69	43.40	43.18	0.16	43.01	43.48	–6.88	0.00
Posterior corneal surface area (mm^2)	44.19	0.31	43.38	44.91	44.31	0.34	43.57	44.79	–5.80	0.00
Total corneal surface area (mm^2)	103.94	1.25	100.80	106.09	103.50	1.20	101.31	105.49	–3.17	0.00
Sagittal plane apex area (mm^2)	4.29	0.25	3.60	4.99	4.02	0.31	3.24	4.86	–9.02	0.00
Sagittal plane area in minimum thickness point (mm^2)	4.30	0.49	0.00	5.01	3.99	0.30	3.22	4.81	–9.01	0.00

(*continued*)

Table 1. (*continued*)

Biometric parameters	Normal group (n = 67)				Subclinical KC group (n = 24)				Z	P
	Mean	SD	Min	Max	Mean	SD	Min	Max		
Anterior apex deviation (mm)	0.00	0.00	0.00	0.01	0.00	0.01	0.00	0.21	–6.01	0.00
Posterior apex deviation (mm)	0.07	0.02	0.02	0.15	0.14	0.07	0.05	0.40	–10.42	0.00
Anterior minimum thickness point deviation (mm)	0.84	0.3	0.42	2.21	1.2	0.29	0.61	1.79	–4.72	0.00
Posterior minimum thickness point deviation (mm)	0.79	0.26	0.46	2.01	1.1	0.29	0.49	1.69	–4.89	0.00
Net deviation from centre of mass XY (mm)	0.05	0.03	0.01	0.09	0.08	0.04	0.00	0.12	–4.20	0.00
Centre of mass X (mm)	0.05	0.03	0.01	0.10	0.04	0.03	0.00	0.08	–3.46	0.28
Centre of mass Y (mm)	0.04	0.03	0.00	0.11	0.01	0.02	0.00	0.10	–7.70	0.14
Centre of mass Z (mm)	0.81	0.02	0.72	0.83	0.78	0.03	0.70	0.81	–0.82	0.08
Volume of corneal cylinder (mm^3) with Radius 0.5 mm	0.47	0.29	0.34	3.21	0.4	0.03	0.29	0.48	–1.02	0.00
Volume of corneal cylinder (mm^3) with Radius 1 mm	1.69	0.13	1.39	1.99	1.49	0.15	1.19	1.9	–1.58	0.00
Volume of corneal cylinder (mm^3) with Radius 1.5 mm	3.89	0.44	3.31	7.29	3.6	0.3	2.9	4.3	–1.9	0.00
Volume of corneal cylinder (mm^3) with Radius 2 mm	7.11	0.45	5.94	8.3	6.55	0.5	5.25	7.8	–2.3	0.00

3.1 Roc Analysis

The predictive value of the modelled parameters was established by a ROC analysis. Six biometric parameters were identified with an area under the ROC (AUROC) above 0.7 (see Fig. 2 and Table 2):

Table 2. Parameters with an AUROC above 0.7

Biometric parameters	AUROC	Sensitivity	Specificity	95% Confidence interval	
				Lower limit	Upper limit
Anterior corneal surface area (mm^2)	0.719	91.5	19.0	0.560	0.779
Posterior corneal surface area (mm^2)	0.701	90.0	20.4	0.521	0.749
Anterior apex deviation (mm)	0.767	67.0	99.9	0.639	0.869
Posterior apex deviation (mm)	0.891	91.6	36.0	0.799	0.959
Anterior minimum thickness point deviation (mm)	0.751	91.4	23.0	0.641	0.849
Posterior minimum thickness point deviation (mm)	0.761	88.1	19.1	0.649	0.858

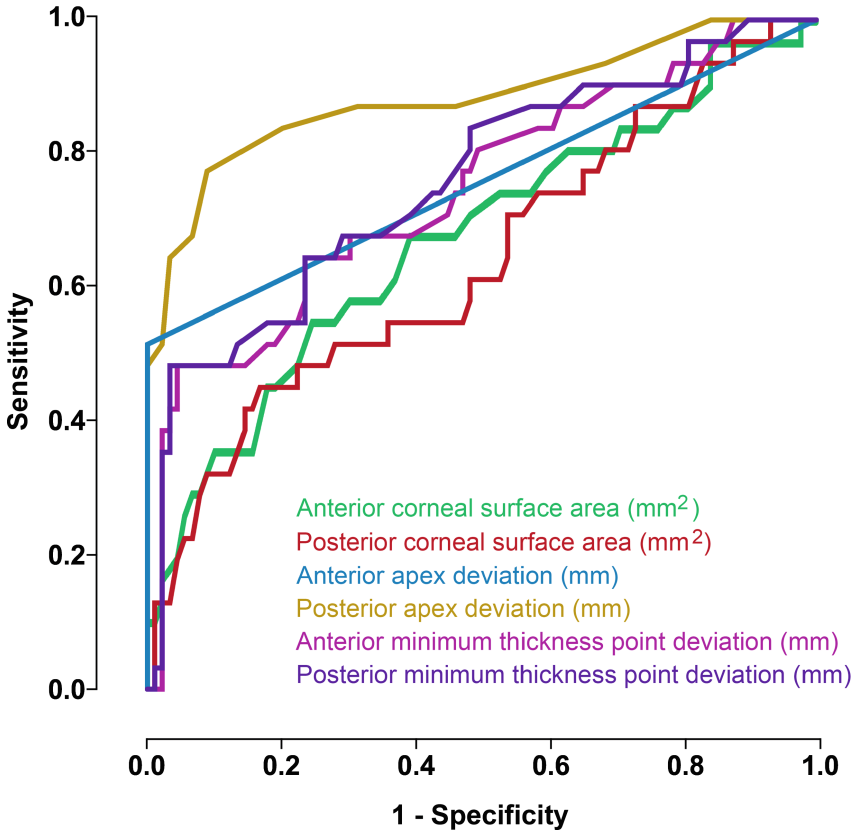

Fig. 2. Curves for modelled parameters detecting subclinical KC with AUROC over 0.7.

4 Discussion

This study obtained good accuracy reconstruction of the intrinsic biometric morphology of the human cornea as a biological structure, making aberrometric analysis unnecessary, and creating a new concise global understanding of early corneal pathology in keratoconic eyes.

The deterioration process in keratoconus is characterized by a significantly reduced total corneal volume compared with healthy eyes, which is triggered by an alteration in corneal collagen fibres that causes stromal thinning and breaks in Bowman's membrane from disease subclinical stages [1]. The studied volumetric parameters and the volume of the analysed corneal cylinders (0.5–1–2 mm) showed a statistically significant reduced total corneal volume in the subclinical group compared with healthy eyes. A similar volumetric reduction of corneas has been described in several studies as a characteristic parameter for the differentiation of subclinical eyes [28–30]. Therefore, the 3D corneal model defined in this work for subclinical keratoconus, allows an accurate characterisation of small changes in its architecture, when the degree of alteration in corneal morphology is low.

Presence of corneal irregularities due to local steepening by a reduced curvature radius leads to increased corneal surface [1]. Eyes with subclinical keratoconus show significant differences for both the anterior and posterior surfaces compared with healthy corneas. In the disease group, these surfaces were larger given their local structural weakening, as fewer collagen fibres are present in each lamella [2]. However, the total cornea area, which included the area of the peripheral region, was larger in healthy corneas, because of their constant thickness compared with the thinning noted in the pathological group due to the influence of intraocular pressure on their weakened structure. This structural weakening is produced by the reduction in the number of stromal lamellae and a reduction in the interconnecting layer's area.

The average distances from the Optical axis to the apex of the anterior and posterior corneal surfaces differed between groups, with the largest deviations found in the group of eyes with subclinical keratoconus. This has been previously described when the disease has been clearly established [1].

The aforementioned presence of an irregular corneal surface, which created a protrusion in the keratoconic eye, also led to incremented corneal curvature [33] and, therefore, to an increase in the deviation distances of corneal apex (maximum curvature) and in the deviation distances of the minimum thickness points, each increase produced in both anterior and posterior surfaces (Table 1). The existence of structural instability in subclinical keratoconic corneas explained why the best disease discrimination results were obtained for the posterior apex deviation variable (ROC area: 0.891, $p < 0.000$, std. error: 0.039, 95% CI: 0.799–0.959). The posterior corneal surface is more susceptible to variations given the forces exerted on tissue [34]. This is why the posterior apex deviation is one of the variables that most reliably represents early changes in patients in first disease stages. Several studies have concluded the importance of, and interest in, the posterior corneal surface [35]. Upon disease onset, structural changes occur on the posterior surface of the cornea, so analysing this surface can positively identify early subclinical keratoconus [29].

Due to all the mentioned above, this new technique could help improve the widely used and well-accepted assessment corneal irregularity methods, in line with the main conclusions drawn by the group of world experts in keratoconus who gathered for the Project "Global Consensus on Keratoconus and Ectatic Diseases" [36]. The existing limitations of current topographic methods (i.e., data interpolation, unknown internal algorithms, etc.) difficult study comparisons and data sharing, and could also lead to relevant information losses. The method proposed in this study is based in a non-finite biometric parameters analysis of the human cornea, and it also does not depend on any restricted commercial algorithm, so could be implemented in all corneal topographers, allowing data comparison between different devices. This technique allows a good and accurate characterization of the corneal health status that will enable new detection paths and to follow-up corneal pathologies.

Funding. This publication has been carried out in the framework of the Thematic Network for Co-Operative Research in Health (RETICS) reference number RD16/0008/0012 financed by the Carlos III Health Institute-General Subdirection of Networks and Cooperative Investigation Centers (R&D&I National Plan 2013–2016) and the European Regional Development Fund (FEDER).

Additional Information

Conflict of Interest: The authors declare no conflict of interest.

Financial Disclosure: Neither author has a financial or proprietary interest in any material or method mentioned.

References

1. Rabinowitz, Y.S.: Keratoconus. Surv. Ophthalmol. **42**, 297–319 (1998)
2. Piñero, D.P., Alió, J.L., Barraquer, R.I., Michael, R., Jimenez, R.: Corneal biomechanics, refraction, and corneal aberrometry in keratoconus: an integrated study. Invest. Ophthalmol. Vis. Sci. **51**, 1948–1955 (2010). https://doi.org/10.1167/iovs.09-4177
3. Egorova, G.B., Rogova, A.: Keratoconus. diagnostic and monitoring methods. Vestn. oftalmol. **129**, 61–66 (2013)
4. Krachmer, J.H., Feder, R.S., Belin, M.W.: Keratoconus and related noninflammatory corneal thinning disorders. Surv. Ophthalmol. **28**, 293–322 (1984)
5. Kennedy, R.H., Bourne, W.M., Dyer, J.A.: A 48-year clinical and epidemiologic study of keratoconus. Am. J. Ophthalmol. **101**, 267–273 (1986)
6. Belin, M.W., Duncan, J.K.: Keratoconus: the ABCD grading system. Klin. Monbl. Augenheilkd. **233**(06), 701–707 (2016). https://doi.org/10.1055/s-0042-100626
7. Amsler, M.: Kératocône classique et kératocône fruste; arguments unitaires. Ophthalmologica **111**, 96–101 (1946). https://doi.org/10.1159/000300309
8. Belin, M.W., Duncan, J., Ambrósio Jr., R., Gomes, J.A.P.: A new tomographic method of staging/classifying keratoconus: the ABCD grading system. Int. J. Kerat. Ect. Cor. Dis. **4**, 55–63 (2015)
9. Cavas-Martinez, F., De la Cruz Sanchez, E., Nieto Martinez, J., Fernandez Canavate, F.J., Fernandez-Pacheco, D.G.: Corneal topography in keratoconus: state of the art. Eye Vis. (Lond) **3**, 5 (2016). https://doi.org/10.1186/s40662-016-0036-8

10. McGhee, C.N., Kim, B.Z., Wilson, P.J.: Contemporary treatment paradigms in keratoconus. Cornea **34**(Suppl 10), S16–S23 (2015). https://doi.org/10.1097/ico.0000000000000504
11. Muftuoglu, O., Ayar, O., Hurmeric, V., Orucoglu, F., Kilic, I.: Comparison of multimetric D index with keratometric, pachymetric, and posterior elevation parameters in diagnosing subclinical keratoconus in fellow eyes of asymmetric keratoconus patients. J. Cataract Refract. Surg. **41**, 557–565 (2015). https://doi.org/10.1016/j.jcrs.2014.05.052
12. Malecaze, F., Coullet, J., Calvas, P., Fournie, P., Arne, J.L., Brodaty, C.: Corneal ectasia after photorefractive keratectomy for low myopia. Ophthalmology **113**, 742–746 (2006). https://doi.org/10.1016/j.ophtha.2005.11.023
13. Ambrosio Jr., R., Dawson, D.G., Belin, M.W.: Association between the percent tissue altered and post-laser in situ keratomileusis ectasia in eyes with normal preoperative topography. Am. J. Ophthalmol. **158**, 1358–1359 (2014). https://doi.org/10.1016/j.ajo.2014.09.016
14. Sonmez, B., Doan, M.P., Hamilton, D.R.: Identification of scanning slit-beam topographic parameters important in distinguishing normal from keratoconic corneal morphologic features. Am. J. Ophthalmol. **143**, 401–408 (2007). https://doi.org/10.1016/j.ajo.2006.11.044
15. Parker, J.S., van Dijk, K., Melles, G.R.: Treatment options for advanced keratoconus: a review. Surv. Ophthalmol. **60**, 459–480 (2015). https://doi.org/10.1016/j.survophthal.2015.02.004
16. Wilson, L.A.B., Humphrey, L.T.: A virtual geometric morphometric approach to the quantification of long bone bilateral asymmetry and cross-sectional shape. Am. J. Phy. Anthropol. **158**, 541–556 (2015). https://doi.org/10.1002/ajpa.22809
17. Bartocci, E., Lio, P.: Computational modeling, formal analysis, and tools for systems biology. PLoS Comput. Biol. **12**, e1004591 (2016). https://doi.org/10.1371/journal.pcbi.1004591
18. Cavas-Martínez, F., Fernández-Pacheco, D.G., De La Cruz-Sánchez, E., Martínez, J.N., Cañavate, F.J.F., Alio, J.L.: Virtual biomodelling of a biological structure: the human cornea. Dyna (Spain) **90**, 647–651 (2015). https://doi.org/10.6036/7689
19. Cavas-Martínez, F., Bataille, L., Fernández-Pacheco, D.G., Cañavate, F.J.F., Alió, J.L.: A new approach to keratoconus detection based on corneal morphogeometric analysis. PLoS ONE **12**(9), e0184569 (2017). https://doi.org/10.1371/journal.pone.0184569
20. Ariza-Gracia, M.A., Zurita, J.F., Piñero, D.P., Rodriguez-Matas, J.F., Calvo, B.: Coupled biomechanical response of the cornea assessed by non-contact tonometry. a simulation study. PLoS ONE **10**, e0121486 (2015). https://doi.org/10.1371/journal.pone.0121486
21. Roy, A.S., Dupps Jr., W.J.: Patient-specific modeling of corneal refractive surgery outcomes and inverse estimation of elastic property changes. J. Biomech. Eng. **133**, 011002 (2011). https://doi.org/10.1115/1.4002934
22. Simonini, I., Pandolfi, A.: Customized finite element modelling of the human cornea. PLoS ONE **10**, e0130426 (2015). https://doi.org/10.1371/journal.pone.0130426
23. Li, X., Yang, H., Rabinowitz, Y.S.: Keratoconus: classification scheme based on videokeratography and clinical signs. J. Cataract Refract. Surg. **35**, 1597–1603 (2009). https://doi.org/10.1016/j.jcrs.2009.03.050
24. Ramos-Lopez, D., et al.: Screening subclinical keratoconus with placido-based corneal indices. Optom. Vis. Sci. **90**, 335–343 (2013). https://doi.org/10.1097/OPX.0b013e3182843f2a
25. Wilson, S.E., Klyce, S.D.: Quantitative descriptors of corneal topography. a clinical study. Arch. Ophthalmol. **109**, 349–353 (1991)

26. Lasko, T.A., Bhagwat, J.G., Zou, K.H., Ohno-Machado, L.: The use of receiver operating characteristic curves in biomedical informatics. J. Biomed. Inform. **38**, 404–415 (2005). https://doi.org/10.1016/j.jbi.2005.02.008
27. Pepe, M.S.: The Statistical Evaluation of Medical Tests for Classification and Prediction. Oxford, New York (2004)
28. Piñero, D.P., Alió, J.L., Aleson, A., Escaf Vergara, M., Miranda, M.: Corneal volume, pachymetry, and correlation of anterior and posterior corneal shape in subclinical and different stages of clinical keratoconus. J. Cataract Refract. Surg. **36**, 814–825 (2010). https://doi.org/10.1016/j.jcrs.2009.11.012
29. Saad, A., Gatinel, D.: Topographic and tomographic properties of forme fruste keratoconus corneas. Invest. Ophthalmol. Vis. Sci. **51**, 5546–5555 (2010). https://doi.org/10.1167/iovs.10-5369
30. Saad, A., Lteif, Y., Azan, E., Gatinel, D.: Biomechanical properties of keratoconus suspect eyes. Invest. Ophthalmol. Vis. Sci. **51**, 2912–2916 (2010). https://doi.org/10.1167/iovs.09-4304
31. Cavas-Martínez, F., Fernández-Pacheco, D.G., Cañavate, F.J.F., Velázquez-Blázquez, J.S., Bolarín, J.M., Alió, J.L.: Study of morpho-geometric variables to improve the diagnosis in Keratoconus with mild visual limitation. Symmetry **10**(8) (2018). https://doi.org/10.3390/sym10080306
32. Cavas Martinez, F., et al.: Detección De Queratocono Temprano Mediante Modelado 3D Personalizado Y Análisis De Sus Parámetros Geométricos. Dyna Ingenieria E Industria **94**(1), 175–181 (2019). https://doi.org/10.6036/8895
33. de Rojas Silva, V.: Clasificación del queratocono. In: Albertazzi, R. (ed.) Queratocono: pautas para su diagnostico y tratamiento. Buenos Aires, Argentina: Ediciones Científicas Argentinas, pp. 33–97 (2010)
34. Sloan Jr., S.R., Khalifa, Y.M., Buckley, M.R.: The location- and depth-dependent mechanical response of the human cornea under shear loading. Invest. Ophthalmol. Vis. Sci. **55**, 7919–7924 (2014). https://doi.org/10.1167/iovs.14-14997
35. Fukuda, S., et al.: Comparison of three-dimensional optical coherence tomography and combining a rotating Scheimpflug camera with a Placido topography system for forme fruste keratoconus diagnosis. Br. J. Ophthalmol. **97**, 1554–1559 (2013). https://doi.org/10.1136/bjophthalmol-2013-303477
36. Gomes, J.A., et al.: Global consensus on keratoconus and ectatic diseases. Cornea **34**, 359–369 (2015). https://doi.org/10.1097/ico.0000000000000408